PROCEEDINGS, 45th Workshop on Geothermal Reservoir Engineering
Stanford University, Stanford, California, February 10-12, 2020
SGP-TR-216

Assessment of Geothermal Energy Extraction from the Mt. Simon Sandstone at University of Illinois at Urbana-Champaign Using a Doublet Well System

Roland Okwen[1], Fang Yang[1], Zhaowang Lin[2], Jiale Lin[2], and Timothy Stark[2]

[1]Illinois State Geological Survey, University of Illinois at Urbana-Champaign, Champaign, IL 61820

[2]Department of Civil & Environmental Engineering, University of Illinois at Urbana-Champaign, Urbana, IL 61801

rokwen@illinois.edu

Keywords: Geothermal reservoir modeling, Wellbore modeling, Doublet well system, Mt. Simon Sandstone, Illinois Basin

ABSTRACT

The presence of low-temperature sedimentary basins in the midcontinent of the United States has spurred interest in utilizing geothermal energy from deep saline aquifers to reduce the use of fossil fuels for direct heating and cooling. However, developing geothermal resources is hindered by high capital cost and risks associated with the feasibility of extracting the resources. To reduce risk and uncertainty in estimating the extractable energy from the Mt. Simon Sandstone (MSS) in the Illinois Basin (ILB), a modeling workflow was developed to assess feasibility of delivering geothermal energy using a two-well (doublet) system. The proposed Deep Direct-Use (DDU) Geothermal Energy System (GES) would directly supply geothermal energy to heat agricultural research facilities (ARF) at the University of Illinois at Urbana-Champaign (U of IL). The total amount of geothermal energy that will be transported to the ground surface was determined by modeling temperature changes from the MSS reservoir to the surface.

A geocellular model informed the reservoir modeling, which was developed with hydraulic and thermal properties measured in boreholes drilled within a 36-square mile (93 km^2) area of around the U of IL. Geothermal reservoir simulations were performed to estimate maximum rates for extracting and injecting the geothermal fluid and evaluate the sensitivity of reservoir temperature distribution with changing the well spacing, extraction and injection rates, and seasonal (ambient ground surface) temperatures. Reservoir modeling results predict maximum extraction and injection rates that greatly exceed the required flow rate of 954 m^3 [6,000 bbl/d] to meet the ARF heating ~2 MMBtu/hour–-and maintain a temperature difference of 11 °C (20 °F) between the extracted and injected fluid.

A 2-D, axisymmetric wellbore model extending from the ground surface to the bottom of the MSS (~1,751 m [5,745 ft] depth) was used to simulate temperature changes during extraction and injection. This model was calibrated to distributed temperature sensing (DTS) log from a CO_2 storage well at the IBDP. The calibrated wellbore model was used to evaluate how variations in the extraction rate, wellbore insulation, and thermal properties of the wellbore materials (i.e., tubing, casing, cement) impact the temperature during extraction. Additionally, the effects of rate, tubing radius, and fluid temperature during injection were investigated. Wellbore modeling results indicated that installing a vacuum-insulated tubing or placing silicate foam around the extraction well tubing would preserve the heat stored in extracted geothermal fluid and limits the temperature change (loss) to <0.6℃ (<1℉). Overall, the temperature change decreased as the extraction and injection rates were increased. Changes in formation heat capacity and tubing radius had negligible effects on the temperature change, whereas the temperature change was reduced as the injection temperatures increased.

Results from reservoir and wellbore modeling indicate that enormous geothermal resource from the MSS can be extracted to meet ARF energy demand. The findings from geothermal reservoir simulations and wellbore modeling informed the design of the surface facilities and doublet well system.

1. INTRODUCTION

This study uses a modeling workflow to assess the feasibility of delivering geothermal energy at flow rates enough to meet the energy demands of Agricultural Research Facilities (ARF) at the University of Illinois (U of IL). Reservoir and wellbore models were constructed to simulate the extraction and injection of MSS geothermal fluid in the Illinois Basin (ILB). A two-well (doublet) system was used in the simulations to deliver and return the fluid to/from the ground surface. Geologic and geocellular models of the MSS developed to characterize the geology of the geothermal reservoir (Lin et al., 2019) provided the hydraulic and thermal properties that were inputted into the model. Changes in fluid temperature in the reservoir were simulated for the 50 years of GES operation. Results of these geothermal reservoir simulations were used to inform the design of the doublet well system.

A wellbore model was constructed to determine the optimal design of the doublet system and estimate changes in fluid temperature along the wellbore during the GES operation. The changes in fluid temperature controls how much geothermal energy can be extracted, and how injection of the fluid would affect temperature in the MSS. An examination of temperature changes (i.e., heat loss or gain) during extraction was made to determine how the thermal properties of geologic formations, insulation methods, and extraction rates impact the overall efficiency of the GES.

2. GEOLOGIC AND GEOCELLULAR MODELING

As a preparatory activity to the geothermal reservoir modeling, a ~93 km^2 (36-square miles) study area centered on the U of IL (Figure 1) was established and far-field geologic features identified that may affect the formation temperature distribution during operation of the GES. The formation-specific hydraulic and thermal properties were compiled from existing drilling and petrophysical logs from the ILB, and laboratory measurements made on core samples. The data included high-resolution downhole temperature measurements from Illinois Basin – Decatur Project (IBDP) collected with a distributed temperature sensing (DTS) system (Schlumberger Carbon Services, 2012) supporting the development of formation-specific thermal gradients (Lin et al. 2019) that were integral to estimating the temperatures of the MSS. The MSS geocellular models were populated with thermal, hydraulic, and mechanical properties that were required for geothermal reservoir modeling. The geocellular model included the Eau Claire Formation, Argenta Formation, and three subzones in the Precambrian basement. Each of these five layers were calibrated with published, average thermophysical and hydraulic properties (e.g., Waples and Waples, 2004). Figures 1a and b show the distributions of porosity and permeability within the MSS model. More information pertaining to the geologic and geocellular models can be found in Lin et al. (2019).

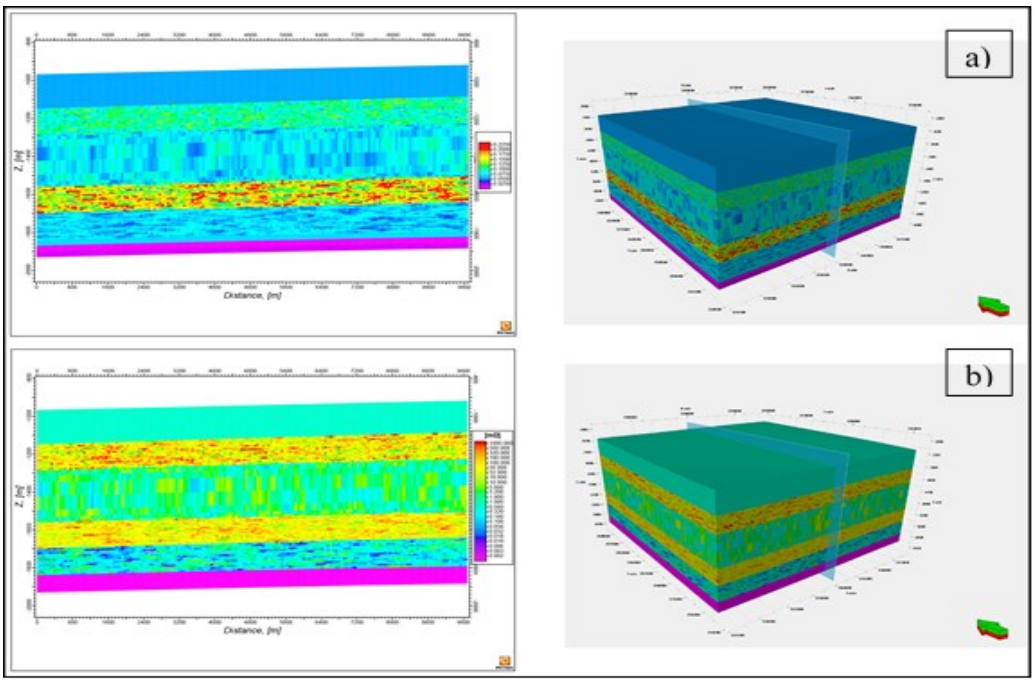

Figure 1: (a) Distribution of porosity and (b) permeability in the Eau Claire formation, MSS (upper, middle, and lower), Argenta formation, and precambrian basement (from top to bottom). x-scale or length: 9656 m (6 miles) and thickness or z-scale: 787 m (2583 ft). Hot colors represent high porosities and permeabilities; cooler colors represent low porosities and permeabilities. the geocellular model was discretized into 159×159×62 finite difference grid cells. Each cell is 61m×61m×12.7m (cell thickness varies, averaging 12.7m). The permeability from the core analysis data from the wells at Decatur and the natural gas storage fields was averaged (9.83 ×10-10 cm2 [99.6 mD]), ranging from 4.93 ×10-15 to 1.46 ×10-8 cm2 (0.0005 to 1480 mD). The porosity was averaged (15.1%), ranging from 0.554% to 31.4%.3.

3. GEOTHERMAL RESERVOIR MODELING

Geothermal reservoir simulations of the MSS were conducted to determine how changes in geothermal fluid temperature impact the efficiency and operation of the GES over a 50-year lifespan. The simulations included varying 1) extraction and injection rates (Table 1), 2) well spacing, 3) injection temperature, and 4) ambient temperature changes at the ground surface (Table 2). Also, the simulations were run to estimate the maximum extraction and injection rates of the doublet well system. The maximum extraction rate was estimated to ensure that sufficient volumes of geothermal fluid could be extracted from the MSS and delivered to meet ARF heating demand. ARF heating demand was estimated based on its energy (propane) consumption to be 2 MMBtu/hr (Lin et al. 2020). The extraction rate required to supply 2 MMBtu/hr of geothermal energy to the ARF is 954 m^3 [6,000 bbl/d]; this is also the targeted injection rate to maintain a temperature difference (ΔT) of 11°C (20°F) (i.e., inflow and outflow temperatures of 43°C [110°F] and 32°C [90°F], respectively). The maximum injection rate was estimated to determine whether extracted geothermal fluid could be injected into the Lower MSS (LMSS) at pressures less than formation parting pressure. As a result, the bottomhole pressure (BHP) of the simulated injection rate was constrained at 90% of the fracture pressure gradient (Table 1) of the MSS based on the fracture gradient of the LMSS at the IBDP site (~16.1 kPa/m [0.71 psi/ft]) (Frailey et al., 2004). The BHP at the extraction well was constrained to 100 psia [689.4857 kPa].

The following assumptions were made in all scenarios:

- the temperature at the bottom confining layer of the MSS is constant,

- the MSS is laterally continuous (i.e., an infinite-acting aquifer),
- the MSS is a normally-pressured formation, and
- all extracted geothermal fluid is injected into the LMSS at the same depth.

A constant temperature boundary condition at the bottom confining layer (i.e., granitic pre-Cambrian formation) assumes continuous, vertically-conductive heat flow from the earth's core through its crust (Grant and Bixley, 2011) into geologic formations that contain geothermal fluids flowing at low velocities. Low velocities provide ample time to heat the aquifer, thus providing more geothermal resources. A laterally continuous assumption means that the MSS can be modeled as an infinite-acting aquifer. Additionally, modeling the MSS as a normally-pressured aquifer assumes that it is at hydrostatic equilibrium with adjacent formations. All scenarios were simulated for a 50 year period, equivalent to or greater than the life span of the DDU GES.

Table 1: Simulations conducted to assess feasibility of delivering geothermal energy from the MSS to ARF at U of IL.

Sensitivity Parameters	Range or Limit	Description
Maximum extraction	BHP at datum (top of model, 100 psia [689.4857 kPa])	Unconstrained brine extraction. Assumption: spatial variation in extraction rate is minimal.
Maximum injection	BHP 90% of fracture gradient	Brine injection (salinity 200,000 ppm). Unconstrained injection rate. Assumption: spatial variation in injection rate is minimal.
Well spacing	0.16 – 3.2 km (0.1 – 2 miles)	Vary extraction -- injection well spacing of between 0.5–2 miles. Using most likely brine extraction rate (954 m^3 [6,000 bbl/d]). It is assumed that all the brine extracted is injected into the MSS.
Extraction rate	5,000 –10,000 bbl/d	Vary extraction rate. Injection rate must be equal to extraction rate to ensure steady state conditions. (1 bbl = 0.158987 m^3)
Return temperature	10–32 ℃ (50–90 ℉)	Vary temperature of fluid prior to injection into the MSS.
Seasonal Temperature Changes	Heating only Heat and cooling	Vary fluid injection temperature to mimic surface temperatures changes in winter, spring, summer, and fall (See Table 2).

Table 2: Season duration and input data used to simulate the effect of seasonal temperature changes.

Season	Period	Heating Scenario		Heating and Cooling Scenario	
		Injection Temperature (°F)	Extraction Temperature (°F)	Injection Temperature (°F)	Extraction Temperature (°F)
Winter	Dec – Apr	50	114	50	114
Spring	May – Jun	70	114	70	114
Summer	Jul – Aug	90	114	140	90
Fall	Sep – Nov	70	114	70	114
***Note**: Extraction rate = 477 m^3/d [3,000 bbl/d] for the summer heating scenario and 954 m^3/d [6,000 bbl/d], for other cases*					

3.1 Reservoir modeling results

Maximum extraction and injection rates:

Reservoir modeling predicted a maximum extraction rate of 3,339 m^3/d (21,000 bbl/d) (Figure 2). The projected maximum injection rate was 1,431 m^3/d (9,000 bbl/d) (Figure 3). Both flow rates are greater than the target rate, and therefore the ARF heating demand can be met. The maximum injection rate is lower than the maximum extraction rate because the pressure change between the injection well and the reservoir was lower than the pressure change between the extraction well and reservoir. For example, the magnitude of the pressure change (Δp), after 50 years of GES operation, of the grid cell at the middle of the perforated interval for the injection well is lower compared to the extraction well (Table 3, first and second row).

Well spacing:

As expected, reservoir modeling predicted lower formation temperatures near the injection well and no temperature change within the vicinity of the extraction well over the lifespan of the GES with a well spacing ≥0.8 km (≥0.5 mile). In addition, a cold temperature (C-T) front developed between the injection and extraction wells. When extraction rate was held constant, the C-T front moved further away from the extraction well as well spacing increased. The C-T front arrived at the extraction well before 50 years when the well spacing is <0.8 km (<0.5 mile) (Figure 4). When the wells were 0.8 km (0.5 mile) apart or greater, temperature change at the extraction well was within 0.6 °C (1 °F) after 50 years of extraction and injection because the C-T front did not breakthrough. A well spacing of 2.4 km (1.5 mile) was considered in subsequent simulations, because it was far enough to avoid unanticipated breakthrough of the C-T front at the extraction well.

Reservoir simulation results show a direct positive relationship between the maximum pressure change and well spacing, but there was no clear correlation between the minimum pressure change and well spacing (Table 3, rows 3-6). Variability in the minimum pressure change may be attributed to differences in the permeability-thickness (kH) product at the extraction well, whose location varies between scenarios.

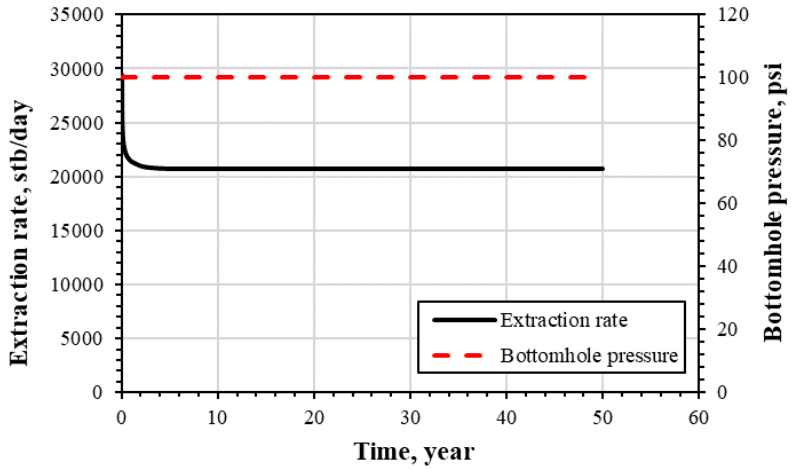

Figure 2: Extraction rate profile at constant extraction BHP (100 psia [689.4857 kPa]).

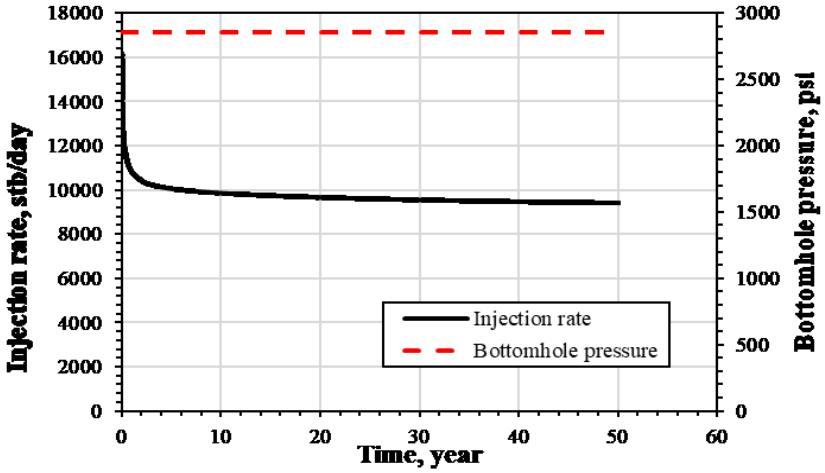

Figure 3: Injection rate profile with injection BHP constrained at 90% of formation fracture pressure.

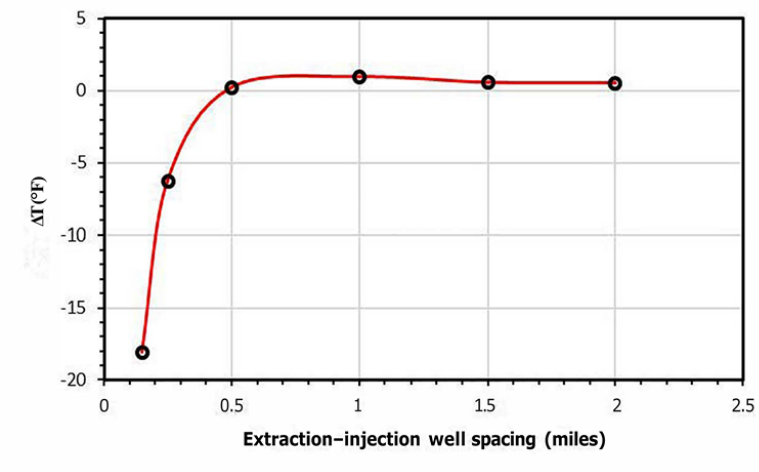

Figure 4: Temperature change (after 50 years) at the mid-perforation of the extraction vs well spacing between the injection and extraction wells. The temperature change at the extraction well is within 1 °F (0.6 °C) when the well spacing is 805 m (0.5 mile).

Table 3: Pressure and corresponding temperature changes after 50 years of GES operation (1 psi = 6.894757 kPa).

Scenario	Case	Pressure change (Δp, psi)		Temperature change (ΔT, °F)	
		Extraction well	Injection well	Extraction well	Injection well
Maximum extraction	Extraction well	-1,181	0	-1.10	1.73
Maximum injection	Injection well	0	643	-54.42	0.54
Well Spacing	0.5 mile	-271	325	-53.43	0.31
	1.0 mile	-431	356	-53.52	0.96
	1.5 miles	-258	371	-53.56	0.58
	2.0 miles	-319	381	-53.59	0.58
Extraction Rate	5,000 bbl/d	-215	306	-53.38	0.48
	6,000 bbl/d*	-258	371	-53.77	0.58
	10,000 bbl/d	-461	624	-54.37	0.96
Injection Temperature	50 °F	-258	413	-63.67	0.58
	60 °F	-258	371	-53.56	0.58
	70 °F	-258	338	-43.47	0.58
	80 °F	-258	311	-33.43	0.58
	90 °F	-258	290	-23.38	0.58
Seasonal Temperature Changes	Heating only	-258	353	-48.05	0.58
	Heating and cooling	-249	351	-52.42	4.49

Extraction rate:

For the same well spacing (1.5 miles), the C-T front moved closer to the extraction well as extraction and injection rates were increased (Figure 5). Although, the pressure change was not the focus of this study, there appears to be a direct relationship between extraction rate and pressure change.

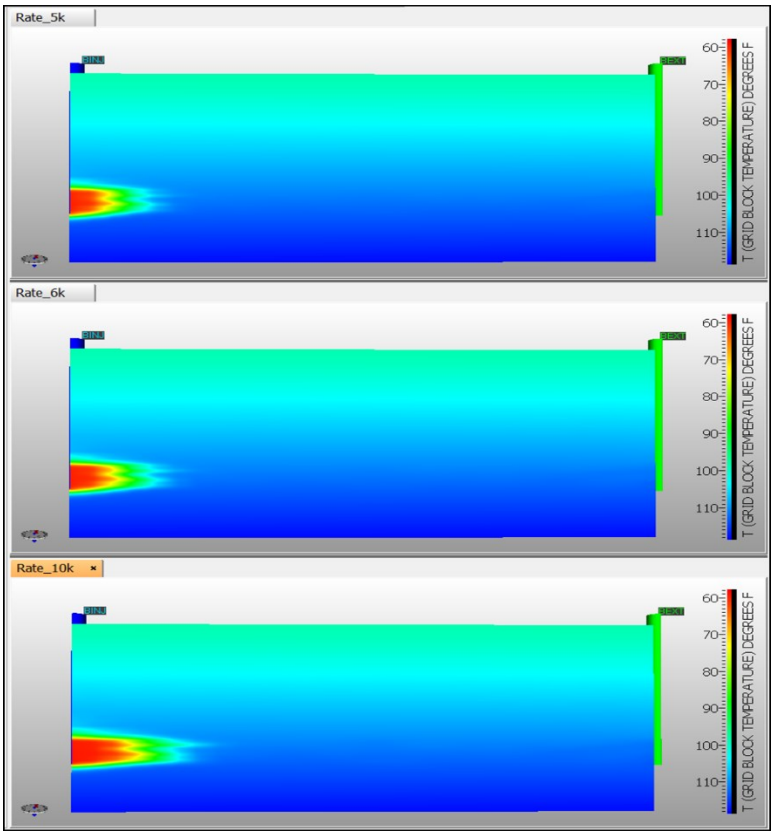

Figure 5: Effect of fluid extract/injection rate on the temperature distribution. Warm colors (near injection well)represent lower temperatures and cooler colors represent higher temperatures. The distance between the extraction well and C-T front decreases with increasing extraction rate (top: 5,000 bbl/d, middle: 6,000 bbl/d, and bottom 10,000 bbl/d). X-scale: 2438 m (8000 ft) and Y-scale: 787 m (2583 ft). Inject well is to the left and extraction well is to the right.

Injection temperature:

The temperature of the extracted geothermal fluid was unaffected by changes in injection temperature prior to breakthrough of C-T front at the extraction well. For example, the temperature change at the center grid cell of the perforated interval of the injection well increased as injection temperature increased, while temperature change at the extraction well remained constant (Table 3). After the C-T front broke through, the temperature of extracted geothermal fluid decreased. Pressure change decreased as injection temperature increased (Table 3), which may be because the viscosity of water decreases with increasing temperature.

Seasonal changes

Changes in injection temperature due to variations in seasonal temperature caused cyclical temperature changes within the vicinity of the injection well. For example, the temperature change of the grid cell at the center of the perforated interval of the injection well decreased by 23–29 ℃ (42–52 ℉) for the 'Heating Only' scenario and about 25–30 ℃ (46–54 ℉) for the 'Heating and Cooling' scenario. The temperature change at the extraction well for the 'Heating Only' scenario remained constant (Figure 6), while cyclical changes (up to 1.7 ℃ or 3.0 ℉) were projected at the extraction well for the 'Heating and Cooling' scenario (Figure 6). The change in temperature at the extraction well for the 'Heating & Cooling' scenario is most likely a result of injecting geothermal fluid (at 60 ℃ or 140 ℉), which is warmer than the formation fluid (at 45.6 ℃ or 114 ℉) during the summer (Table 2).

Seasonal changes in extraction and injection rates for both the 'Heating Only' and 'Heating and Cooling' scenarios (Table 2) caused cyclical changes in pressure near the extraction and injection wells, especially for the 'Heating and Cooling' scenario (Figure 6). The large fluctuations in pressure at the extraction and injection wells for the 'Heating and Cooling' scenario (Figure 6) are most likely due to reversing the direction of fluid flow (i.e., wells switched from extraction to injection and vice versa) to provide cooler fluid during the summer (Table 2).

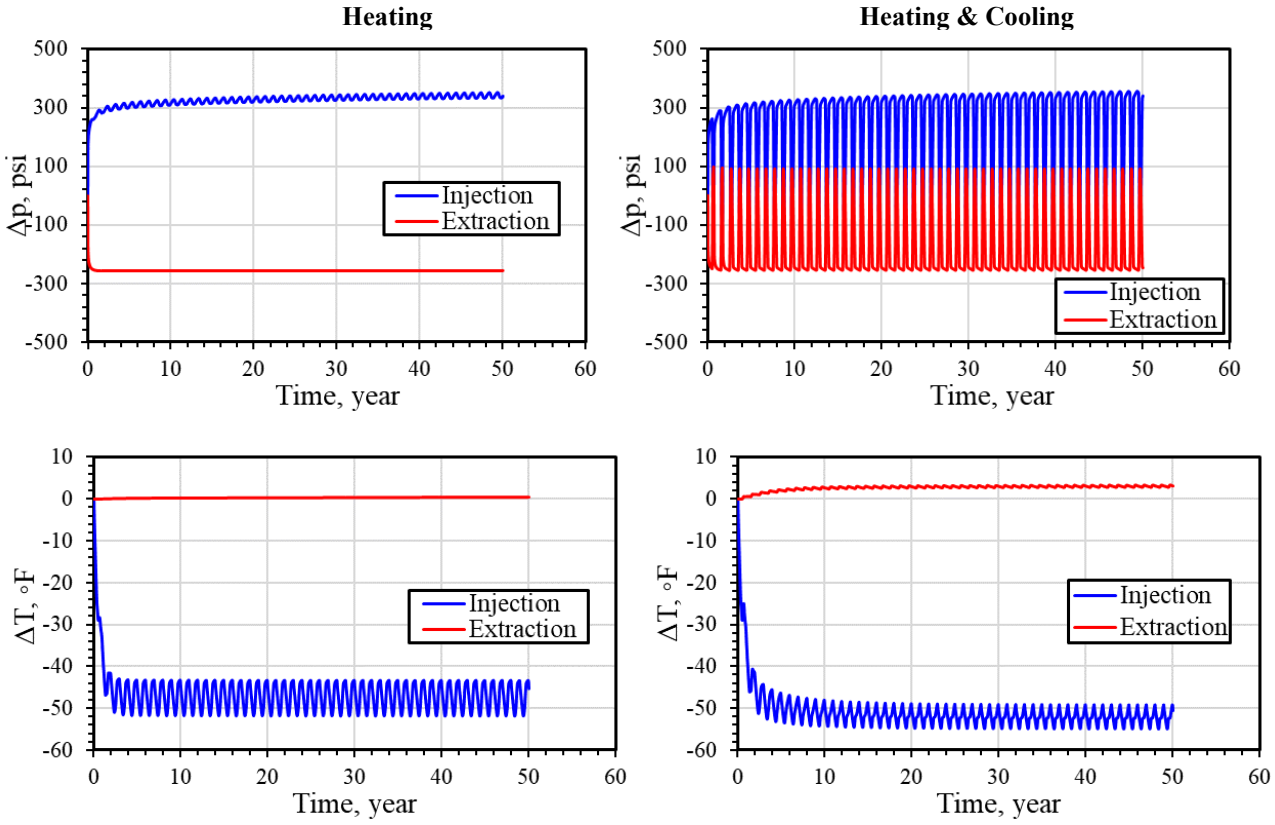

Figure 6: Effect of seasonal changes in temperature for 'Heating Only' and 'Heating and Cooling' scenarios (50 years). Temperature changes at the extraction well are relatively small. Pressure changes at the extraction and injection wells are relatively large (~300 psi).

3.2 Wellbore Modeling

Temperature change between the wellbore and adjacent formations or between the reservoir and surface (or vice versa) was estimated via finite element modeling. The COMSOL Multiphysics (version 5.3) software package was used to simulate temperature changes during extraction and injection.

A representative thermal gradient in the ILB located in the study area was necessary to estimate formation temperatures and, ultimately, temperature change during extraction and injection. Thermal gradients (from ground surface to the Precambrian basement) that were

estimated from continuous downhole temperature measurements taken at the IBDP site using a distributed temperature sensing (DTS) system (Schlumberger Carbon Services, 2012) were used to develop a temperature profile (Figure 7) of the MSS at the U of IL study site (Lin et al. 2019). The temperature of the MSS ranged between 39°C–46°C (102°F–114°F; sky blue line in Figure 7).

Geometry and boundary conditions:

A 2-D, axisymmetric wellbore model was used to simulate heat transfer along the extraction and injection wellbores (Figure 8). The wellbore model extends from the surface to the bottom of the MSS (1,887 m [6,191 ft]), representing 17 geologic formations. A model width of 50.3 m (165 ft) – significantly larger than the casing diameter (0.178 m [7.0 in]) – was used to minimize boundary effects. The model was discretized using a finite element mesh consisting of 96,798 mapped, structured quadrilateral elements. The average thermal properties, hydraulic parameters, and petrophysical data used to parameterize the wellbore model (Table 4) were drawn from the literature–either from measurements from the ILB (Leetaru, 2014; Freiburg et al., 2016; Panno et al., 2013; Anovitz et al., 2018; Ritzi et al., 2018) or from data for similar geologic formations (Freeze and Cherry, 1979; Morrow et al., 2017; Robertson, 1988; Schön, 2015; Waples and Waples, 2004; Walker et al., 2015). Additionally, average geothermal properties from the geocellular model, such as thermal conductivity, specific heat capacity, and thermal expansion coefficient that were modeled from overall quartz content and temperature were used as inputs in the wellbore model.

Wellbore materials:

Thermal and physical properties of the wellbore materials are presented in Table 5. These properties were considered as a baseline case (i.e., the wellbore without insulation) and were used to assess the performance of two wellbore insulation methods (i.e., silicate foam and vacuum-insulated tubing). All thermal properties of the wellbore components (i.e., tubing, casing, cement) were assumed to be unaffected by changes in temperature in all modeled scenarios.

Model calibration:

Thermal gradients derived from DTS data were calibrated to BHT measurements taken from shallower wells located near U of IL. Specifically, the trend lines from the DTS measurements were adjusted (by fine tuning thermal conductivity), to match the BHT of each well, starting with the measured temperature profile of the IBDP site. To develop the temperature profile from the surface to LMSS, one BHT was selected for each formation interval to represent the regional temperature. The simulated temperature profile at the ARF (red dash line in Figure 7), which closely matched the temperature profile derived from DTS data, was used to calculate the initial temperature along the wellbore at the ARF.

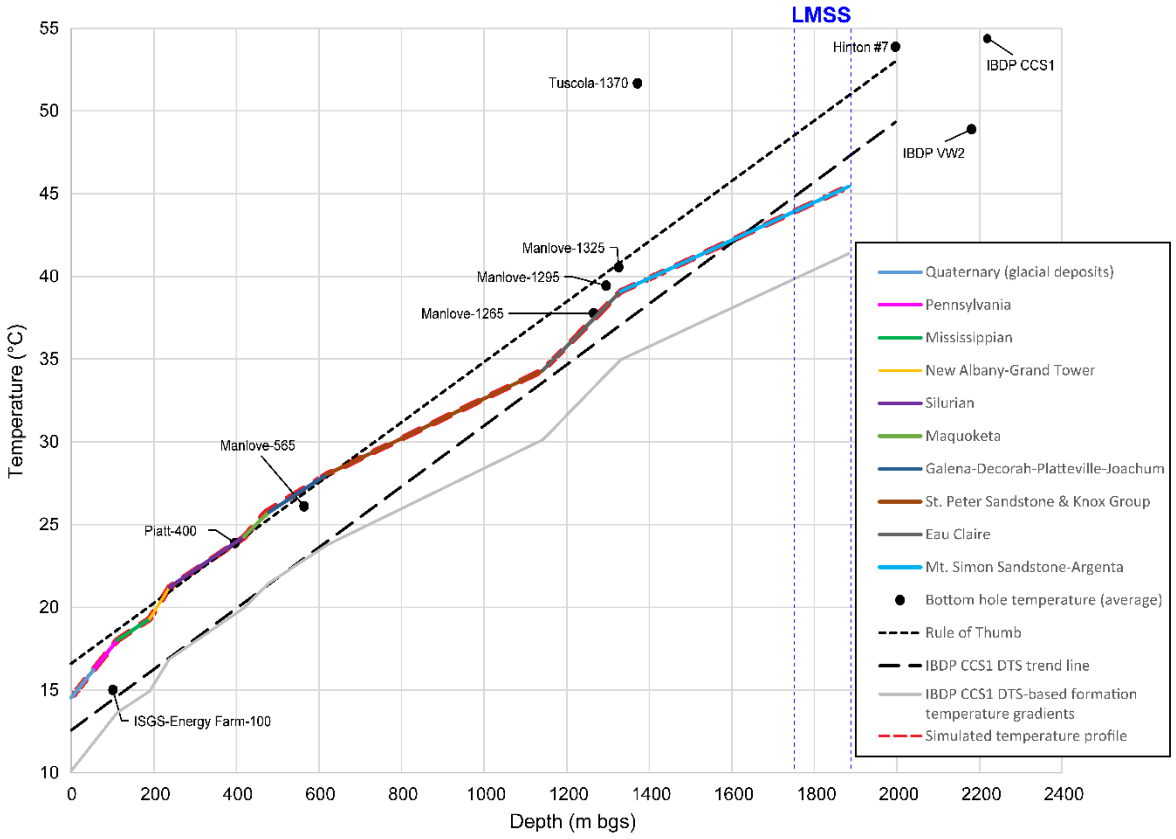

Figure 7: Measured and COMSOL calculated (short dashes) temperature profiles for the ARF that were used in wellbore modeling.

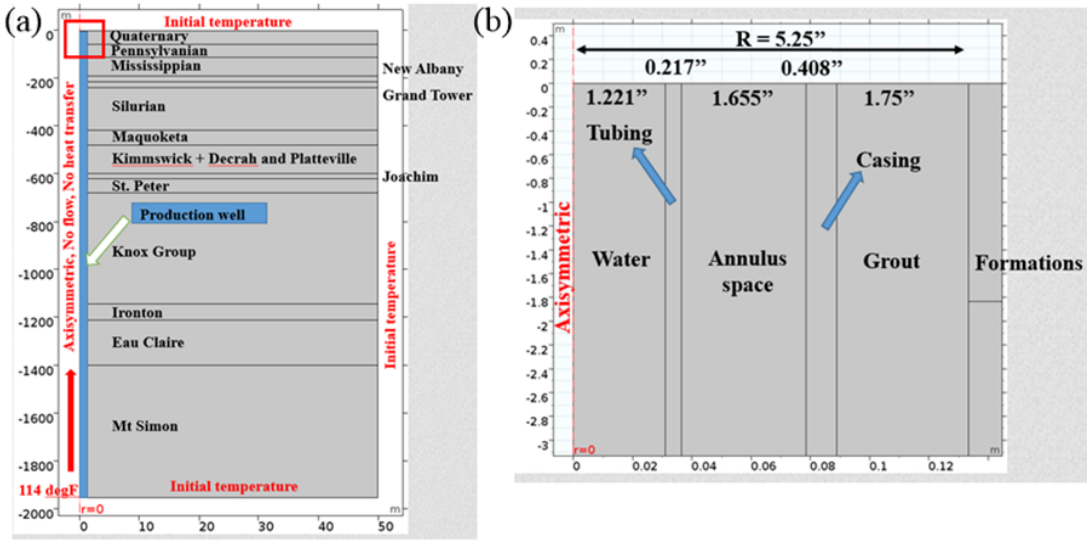

Figure 8:Wellbore modeling geometry and boundary conditions for: (a) axisymmetric wellbore model with boundary conditions and (b) wellbore components (1" = 0.0254 m).

Table 4. Thermal properties, hydraulic parameters, and petrophysical data of various Geologic Formations

Unit	Thickness (ft)	Density (g/cm3)	Porosity	Permeability (mD)	Heat Capacity (J/kgK)	Thermal Conductivity (W/mK)
Soil	6	1.085	0.400	50	2530	1.57
Quaternary 1	80.5	2.4	0.250	2	545	2.21
Quaternary 2	103.5	1.635	0.380	9000	2380	2.31
Pennsylvanian	175	2.48	0.120	5	1010	1.84
Mississippian	257	2.66	0.150	10	820	3.5
New Albany	79	2.54	0.200	0.01	879.2	1.3
Grand Tower (Devonian)	79	2.71	0.140	12	921	1.5
Silurian	590	2.8	0.120	1	879.2	3.5
Maquoketa (Ordovician)	200	2.54	0.200	0.01	863	2.3
Kimmswick	127	2.71	0.140	10	921	3.8
Decorah and Platteville	270	2.71	0.140	10	921	3.8
Joachim	63	2.7	0.130	2	900	4.2
St. Peter	195	2.67	0.167	163	825	3.3
Knox Group	1400	2.71	0.070	4	921	4.9
Ironton	125	2.67	0.045	0.4	820	3.5
Eau Claire	616	2.6	0.058	0.65	795	2.3
Mt. Simon	1814	2.67	0.125	92	820	5.1

Wellbore simulation scenarios:

The wellbore model was used to simulate the effects of extraction rate, wellbore insulation, and the material properties of wellbore components (i.e., tubing, casing, cement, annulus fluid) on temperature change during extraction and injection. All material properties of the wellbore components (Table 5) were assumed to be unaffected by changes in temperature in all simulations. The baseline case simulated the estimated extraction rate needed to meet ARF energy demand (954 m^3 [6,000 bbl/d]) with no wellbore insulation (Tables 6 and 7).

Two wellbore insulation methods were simulated: (1) silica foam placed around the wellbore tubing and (2) a vacuum-insulated two-layered tubing (Table 6). The thermal conductivity of wellbore components (i.e., grout, annulus fluid, tubing, and casing) were used to simulate the two insulation methods (Table 7). Injection well insulation was not simulated because the temperature of the geothermal fluid discharged from surface facilities would be lower than the temperature of the LMSS (except during cooling), where it will be returned. Instead, scenarios to determine how injection rate and tubing radius affect temperature change during injection were simulated.

Table 5. Material properties of wellbore components – Baseline Case

Material Property	Tubing and casing	Grout	Annulus fluid
	Carbon steel (API N-80 grade)	Type I Portland cement (ASTM C 150)	Potassium formate brines (weight concentration = 75%)
Thermal conductivity (W/m.K)	55	0.80	0.38
Density (kg/m^3)	7850	1498 (surface to 6000ft) 1893 (6000ft to bottom)	1522
Solid specific heat (J/kg.K)	510	2000	1380

Table 6. Wellbore simulations performed to assess feasibility of delivering geothermal energy from the MSS to ARF at U of IL.

Scenario	Case	Description
Extraction Well		
Extraction rate (no insulation)	715 m^3/d (6,000 bbl/d)	Baseline extraction rate
	1,192 m^3/d (10,000 bbl/d)	
Wellbore insulation	Silicate foam	Foam is wrapped around the tubing Extraction rate: 6,000 bbl/d
	Vacuum-insulated tubing	Two layered tubing. Extraction rate: 6,000 bbl/d
Heat capacity (C_p) sensitivity	0.1 C_p 1 C_p 10 C_p	-
Injection Well		
Injection rate	2.4 -1,192 m^3/d	20 -10,000 stb/d
Tubing radius	0.02 m, 0.03 m, and 0.04 m	0.9 in, 1.22 in*, and 1.5 in
Note: * 1.22 in tubing radius are commonly used. 0.9 in and 1.5 in radii were used for comparison purpose		

Table 7. Thermal conductivity of different extraction well insulation scenarios and wellbore parameters

Insulation Scenario	Grout	Annulus fluid	Carbon Steel tubing: OD = 0.073 m Casing: OD = 0.178 m
	Type I Portland cement (ASTM C 150) (W/m.K)	Potassium formate brines (wt. % = 75) (W/m.K)	(W/m.K)
Baseline (No insulation)	0.80 (Allen and Philippacopoulos, 1999)	0.38 (CABOT, 2019)	55 (National Physical Laboratory, 2017)
Extraction Well (Silicate foam around tubing)	0.80	0.104 (Penberthy and Bayless, 1974)	55
Vacuum-Insulated Tubing (Tubing has two layers and vacuum between layers)	0.80	0.38	0.06 (Sliwa and Kruszewski, 2017)

Wellbore modeling results:

Wellbore modeling results for extraction rate, wellbore insulation, and heat capacity sensitivity simulations are presented in Figure 9 and Figure 10. Wellbore modeling projected temperature change along the wellbore to increase with decreasing extraction rate. Moreover, wellbore modeling results also indicate that temperature change could be reduced to less than 0.6 ^oC (1 ^oF) by insulating the wellbore or increasing brine extraction rate. Increase in temperature change with decreasing extraction rate is most likely due to a corresponding increased contact between the extracted brine and wellbore, thus providing ample time for heat transfer, via conduction, to formations surrounding the wellbore. Additionally, the modeling results presented in Figure 7 suggest that placing silicate foam around the tubing is more effective in insulating the wellbore than using a vacuum-insulated tubing. However, the difference in temperature change between the two insulation methods is not significant (i.e., less than 0.3 ^oC or 0.5 ^oF). As a result, both methods could be suitable for wellbore insulation. Lastly, the results presented in Figure 10 indicate that temperature change along the wellbore is relatively insensitive to changes in the heat capacity of adjacent geologic formations, especially at high temperatures (or depths, Figure 10).

On the other hand, Figure 11 and Figure 12 present wellbore modeling results for geothermal fluid injection rate and tubing radius. Contrary to extraction modeling results, injection modeling results predict temperature change to increase with decreasing injection rate (Figure 11). The decrease in temperature at shallow depths and low injection rates, depicted in Figure 11, is most likely because the formation temperature is less than brine injection temperature, thus causing brine to loss heat via conduction and convection. However,

brine gained more heat at lower rates and greater depths as formation temperature increasingly become higher than temperature of the injected geothermal fluid (Figure 11).

Contrary to injection rate, tubing radius correlated positively with temperature change (i.e., temperature change increased with increasing tubing size), at constant rate. The temperature change increased with tubing radius because large tubing radii provide wider surface areas for heat transfer from the surrounding geologic formations to the injected geothermal fluid. However, temperature change for the three tubing size cases are essentially the same.

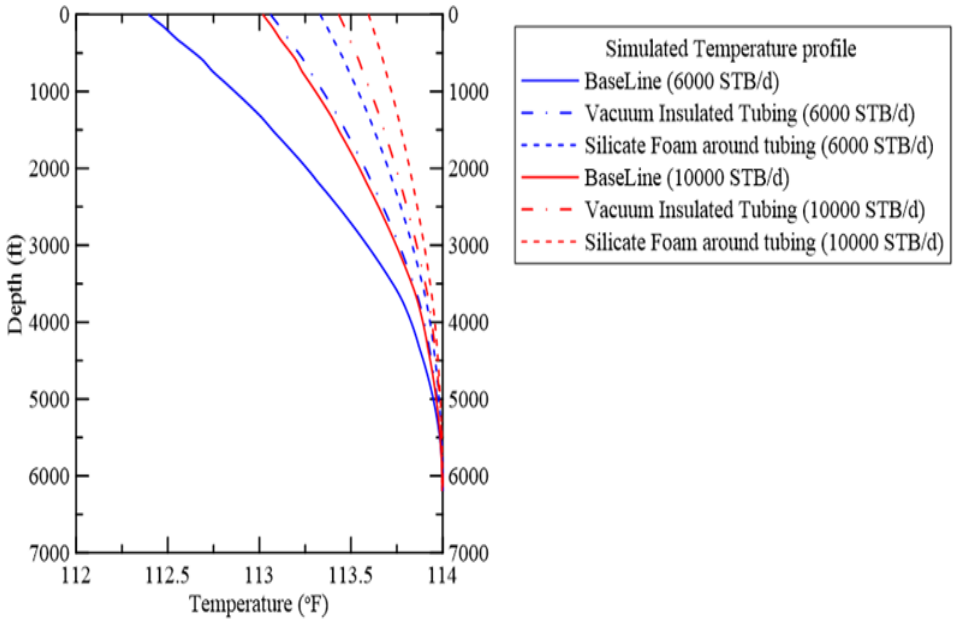

Figure 9: Temperature profiles along the center line of extraction well for different flow rates and wellbore insulation methods (122 - 114 ^{o}F = 44.4 - 45.6 ^{o}C and 1 bbl/d = 0.158987 m^{3}).

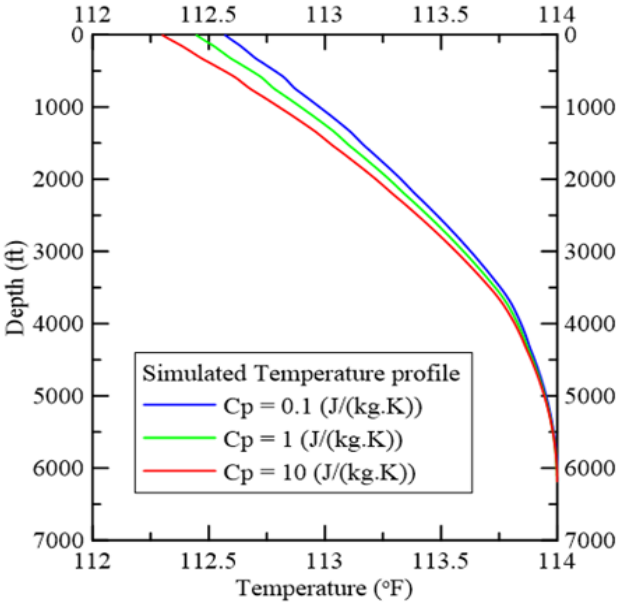

Figure 10: Temperature profiles along the center line of extraction well for different formation heat capacities (122 - 114 ^{o}F = 44.4 - 45.6 ^{o}C).

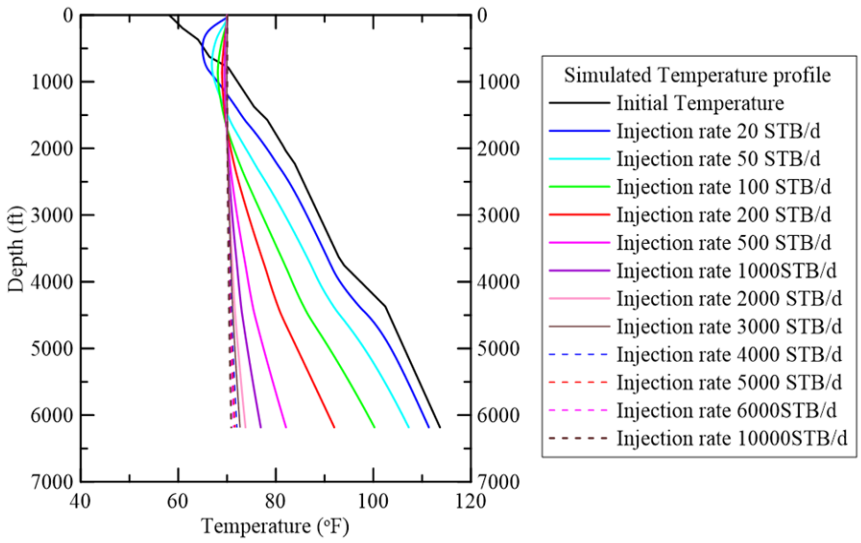

Figure 11: Temperature profiles using different injection rates and an initial injection temperature of (T_{inj}) of 21.1 ^{o}F (70 ^{o}F) [122 - 114 ^{o}F = 44.4 - 45.6 ^{o}C and 1 bbl/d = 0.158987 m^3].

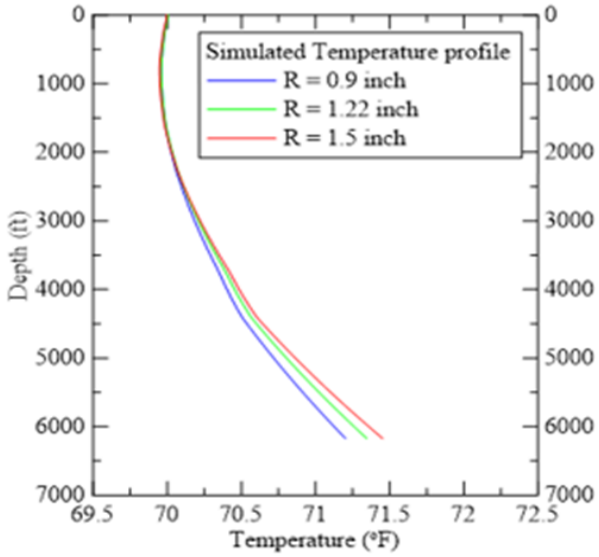

Figure 12: Temperature profile along the center line of the injection wellbore for different tubing radius with constant injection rate. R = tubing radius (1" = 0.0254 m).

4. CONCLUSIONS

This study exemplifies a modeling approach that can be successfully conducted to assess the feasibility of Deep Direct-Use Geothermal Energy System applications in the ILB. Together, geothermal reservoir and wellbore modeling results demonstrate that the two-well (doublet) system can supply geothermal heat from the MSS to the ARF at sufficient flow rates to meet ARF energy demand.

Geothermal reservoir simulations show that the doublet well system can deliver a maximum extraction rate of 3,180 m^3/d (20,000 bbl/d) and a maximum injection rate of 1,431 m^3/d (9000 bbl/d), which exceeds the required extraction and injection rate of 954 m^3/d (6,000 bbl/d). Results also show that a cold-temperature front will develop near the injection well because geothermal fluid will be injected into the LMSS at a temperature less than reservoir temperature. In addition, simulation results suggest that injection-extraction well spacing should be greater than 0.8 km (0.5 mile) to avoid breakthrough of the cold temperature front at the extraction well.

A finite element wellbore model was used to simulate temperature changes along the wellbore during extraction and injection. Modeling results suggest that insulating the wellbore by placing silicate foam around the extraction well tubing or installing a vacuum-insulated tubing could minimize temperature loss during extraction to less than 0.6^{o}C (1^{o}F).

ACKNOWLEDGEMENTS

This material is based on work supported by the U.S. Department of Energy's Office of Energy Efficiency and Renewable Energy (EERE) under Geothermal Technologies Office Award Number DE-EE0008106.

Through a university grant program, IHS Petra, Geovariances Isatis, COMSOL Group, Inc., and Landmark Software were used for the geologic, geocellular, wellbore, and reservoir modeling, respectively.

REFERENCES

Allen M.L and Philippacopoulos A.J. (1999). Properties and performance of cement-based grouts for geothermal heat pump applications. Office of Geothermal Technologies United States Department of Energy Washington, DC 20585.

Anovitz, L.M., J.T. Freiburg, M. Wasbrough, D.F.R. Mildner, K.C. Littrell, V. Pipich, and J. Ilavsky.: The Effects of Burial Diagenesis on Multiscale Porosity in the St. Peter Sandstone: An Imaging, Small-Angle, and Ultra-Small-Angle Neutron Scattering Analysis. Marine and Petroleum 92: 4352–4371 (2018). https://doi.org/10.1016/j.marpetgeo.2017.11.004.

Formate Technical Manual (CABOT). Retrieved at http://www.cabotcorp.com/solutions/products-plus/cesium-formate-brines/formate-technical-manual

Freeze, R.A., and J.A. Cherry.. Groundwater. Englewood Cliffs, New Jersey: Prentice-Hall Incorporated (1979).

Freiburg J.T., R.W. Ritzi, and K.S. Kehoe.. Depositional and Diagenetic Controls on Anomalously High Porosity within a Deeply Buried CO2 Storage Reservoir the Cambrian Mt. Simon Sandstone, Illinois Basin, USA. International Journal of Greenhouse Gas Control 55: 42–54 (2016). https://doi.org/10.1016/j.ijggc.2016.11.005.

Frailey, S.M., J.P. Grube, B. Seyler, and R.J. Finley.: Investigation of Liquid CO2 Sequestration and EOR in Low Temperature Oil Reservoirs in the Illinois Basin. Presented at SPE/DOE 14th Symposium on Improved Oil Recovery. Tulsa, OK, April 17–21, 2004. Society of Petroleum Engineers. SPE-89342-MS. https://doi.org/10.2118/89342-MS.

Grant, M.A. and Bixley, P.F., 2011. Geothermal Reservoir Engineering. Copyright © 2011, Elservier Inc. ISBN: 978-0-12-810375-3

Leetaru, H.E.: An Evaluation of the Carbon Sequestration Potential of the Cambro-Ordovician Strata of the Illinois and Michigan Basins. Champaign, IL: Illinois State Geological Survey (2014). DOE-DE- FE0002068 Final Report. https://doi.org/10.2172/1167490. http://hdl.handle.net/2142/95114.

Lin, Y. -F., Stumpf, A. J., Frailey, S. M., & Holcomb, F. H.: Feasibility of Deep Direct-Use Heating for District-Scale Energy Systems over the Illinois Basin, Abstracts with Programs, Geological Society of America, Phoenix, AZ, 51(5), (2019), http://dx.doi.org/10.1130/abs/2019AM-337671.

Morrow C.A., J.O. Kaven, D.E. Moore, and D.A. Lockner.: Physical Properties of Sidewall Cores from Decatur, Illinois. Reston, VA: U.S. Geological Survey (2017). Open-File Report 2017-1094. https://doi.org/10.3133/ofr20171094

National Physical Laboratory. Retrieved at http://www.kayelaby.npl.co.uk/general_physics/2_3/2_3_7.html

Panno S.V., K.C. Hackley, R.A. Locke, I.G. Krapac, B. Wimmer, A. Iranmanesh, and W. Kelly.: Formation Waters from Cambrian-Age Strata, Illinois Basin, USA: Constraints on their Origin and Evolution."". Geochimica et Cosmochimica Acta 122: 184–197 (2013). https://doi.org/10.1016/j.gca.2015.06.013.

Ritzi, R.W., R. Ghose, M. Bottomley, A.J.H. Reesink, J. Best, J.T. Freiburg, and N.D. Webb. : Linking the Local Vertical Variability of Permeability and Porosity to Newly-Interpreted Lithofacies in the Lower Mt. Simon CO2 Reservoir. International Journal of Greenhouse Gas Control 68, (2018), 26–41. https://doi.org/10.1016/j.ijggc.2017.09.017.

Robertson, E.C.: Thermal Properties of Rocks. Reston, VA: U.S. Geological Survey, Open-File Report 88-441 (1988). https://pubs.usgs.gov/of/1988/0441/report.pdf.

Schön, J.H.: Thermal properties (Chapter 9). In Physical Properties of Rocks – Fundamentals and Principles of Petrophysics. Developments in Petroleum Sciences 65, (2015), 369–414. http://dx.doi.org/10.1016/b978-0-08-100404-3.00009-3

Schlumberger Carbon Services.: Deep Well Monitoring and Verification at the Illinois Basin Decatur Project (Slide 12). Presented at Midwest Geological Sequestration Consortium Annual Meeting, September 18, (2012). http://www.sequestration.org/resources/PAGSept2012Presentations/06-JimKirksey_PAG2012.pdf

Waples D.W., and J.S. Waples. : A Review and Evaluation of Specific Heat Capacities of Rocks, Minerals, and Subsurface Fluids (Part 1: Minerals and nonporous rocks). Natural Resources Research 13(2), (2004) 97–122. https://doi.org/10.1023/B:NARR.0000032647.41046.e7.

Walker, M.D., L.L. Meyer, J.M. Tinjum, and D.J. Hart.: Thermal Property Measurements of Stratigraphic Units with Modeled Implications for Expected Performance of Vertical Ground Source Heat Pumps. Geotechnical and Geological Engineering 33(2), (2015), 223–238. https://doi.org/10.1007/s10706-015-9847-y